

# Interplay between writhe and knotting for swollen and compact polymers

Marco Baiesi,<sup>1,2,\*</sup> Enzo Orlandini,<sup>2,3,†</sup> and Stuart G. Whittington<sup>4,‡</sup>

<sup>1</sup>*Instituut voor Theoretische Fysica, K.U.Leuven, Celestijnenlaan 200D, 3001, Belgium.*

<sup>2</sup>*Dipartimento di Fisica, Università di Padova, Via Marzolo 8, 35131 Padova, Italy*

<sup>3</sup>*INFN, Sezione di Padova, Via Marzolo 8, 35131 Padova, Italy*

<sup>4</sup>*Department of Chemistry, University of Toronto, Toronto, Canada M5S 3H6*

The role of the topology and its relation with the geometry of biopolymers under different physical conditions is a nontrivial and interesting problem. Aiming at understanding this issue for a related simpler system, we use Monte Carlo methods to investigate the interplay between writhe and knotting of ring polymers in good and poor solvents. The model that we consider is interacting self-avoiding polygons on the simple cubic lattice. For polygons with fixed knot type we find a writhe distribution whose average depends on the knot type but is insensitive to the length  $N$  of the polygon and to solvent conditions. This “topological contribution” to the writhe distribution has a value that is consistent with that of ideal knots. The standard deviation of the writhe increases approximately as  $\sqrt{N}$  in both regimes and this constitutes a geometrical contribution to the writhe. If the sum over all knot types is considered, the scaling of the standard deviation changes, for compact polygons, to  $\sim N^{0.6}$ . We argue that this difference between the two regimes can be ascribed to the topological contribution to the writhe that, for compact chains, overwhelms the geometrical one thanks to the presence of a large population of complex knots at relatively small values of  $N$ . For polygons with fixed writhe we find that the knot distribution depends on the chosen writhe, with the occurrence of achiral knots being considerably suppressed for large writhe. In general, the occurrence of a given knot thus depends on a nontrivial interplay between writhe, chain length, and solvent conditions.

PACS numbers: 02.10.Kn, 36.20.Ey, 87.15.A-, 36.20.-r

## I. INTRODUCTION

Important biopolymers such as duplex DNA exist as double-stranded macromolecules, where the two strands of complementary nucleotides are wound around each other in a right-handed fashion and around a common axis [1]. In addition, the double helix can wind in space to form a new super-helix, in which case the polymer is said to be supercoiled. A geometric quantity that has proved to be useful in describing the degree of supercoiling in double stranded DNA (dsDNA) is the writhe of a curve, and there is an important conservation theorem [2, 3] relating the writhe of the central axis of circular dsDNA to the double helical twist and the linking number of the two strands. Supercoiling in DNA can result from its binding to proteins (histones) in chromatin or from a linking deficit between the two strands, when the macromolecule becomes a ring, for instance by cyclization. For example, circular DNA extracted from cells has negative supercoiling [4]. On the other hand random cyclization of linear dsDNA with cohesive ends can trap DNA topoisomers as knots [5, 6]. Both supercoiling and knotting in circular DNA are critical to the functioning of the cell [7] and, for this reason, there exist enzymes to control the writhe and the knotting of DNA, especially during replication, transcription and recombination. This sug-

gests that supercoiling and knot formation are relevant indicators of the spatial arrangement of circular DNA and that a detailed study of their reciprocal influence is crucial in understanding the conformational properties of this macromolecule at equilibrium [8, 9].

A relationship between writhe and knot type is evident also in the knot theory of random closed curves where it is known for example that chiral knots have a non negligible writhe whose sign depends on the chirality of the knot, and that there are families of knots (e.g. torus and twist knots) that can be clearly distinguished in terms of their average writhe [10, 11]. For physical knots this relationship is more stringent and allows a classification of knots in terms of the geometrical (writhe) properties of their ideal representations [11, 12, 13].

The above mentioned examples refer in general to situations in which the polymer is in a swollen phase due to good solvent or unconstrained conditions. There are however several important cases in which macromolecules such as DNA and proteins are in highly condensed phases due to bad solvent conditions or to strong confinement. Highly compact configurations have geometrical properties that clearly differ from their swollen counterparts and this may change the relationship between writhe and knotting quite dramatically. This is the case, for example, for highly condensed DNA extracted from P4 phages [14, 15, 16, 17, 18]. The genome of the P4 phage is a linear dsDNA, about 11 Kbp long and having two 19bp single stranded cohesive ends [19]. In P4 tailless mutants the two ends can move freely within the capsid and at the end of the packing process they can cohere to form rings. Since the genome is very long compared to the

\*baiesi@pd.infn.it

†orlandini@pd.infn.it

‡swhittin@chem.utoronto.ca

linear size of the capsid (50nm) the DNA is very condensed and a high probability of knotted molecules is expected. The experimental data show that over 97% of the molecules in tailless mutants are indeed knotted. This is dramatically higher than the 3% value observed when P4 DNA molecules undergo cyclization in free solution [6, 20]. Moreover, knots in P4 phages are very complex, being characterized by a crossing number often much greater than 10 [17]. A more detailed analysis of the extracted knot spectrum based on 2D gel electrophoresis reveals a predominance of chiral knots over achiral ones and a prevalence of torus knots over twist knots [18, 21]. These findings suggest a spatial organization of the viral genome characterized by a large amount of writhe that induces a bias in the observed knot spectrum towards chiral and, especially, torus knots [18, 21]. This may suggest an important contribution of the writhe to the condensation of DNA [22].

All the examples outlined above suggest the importance of a theoretical study of the interplay between writhe and knot distribution for polymer rings under different equilibrium conditions. Here we explore the relation between writhe and knotting for the two extreme cases of polymers in the swollen and compact phases.

We perform Monte Carlo simulations on a simple discrete model of a self-attracting ring polymer, namely a polygon in the cubic lattice in which the quality of the solvent is mimicked by assigning an energy gain to any pair of nearest neighbor non-consecutive vertices of the polygon. By tuning properly the energy gain this model is known to describe a collapse ( $\Theta$ ) transition from a swollen phase, characterized by extended configurations, to one in which the polygons are compact [23, 24, 25]. This allows us to compare, within the same model, the relationship between writhe and knotting in the two regimes and to see, for example, to what extent the degree of condensation of the polymer affects the writhe distribution and its relation to the knot spectrum.

The plan of this paper is as follows. In the next section we describe the model, the Monte Carlo algorithms and the techniques adopted to compute the writhe and to identify the knot type. In Sec. III we present the results first for the writhe distribution at fixed knot type and then for the knot spectrum as a function of the writhe. Section IV is devoted to a general discussion of the results presented and to some conclusions.

## II. MODEL AND SIMULATION METHODS

### A. Polymer model

As a model for the large scale behavior of a long flexible circular polymer in a good solvent (*swollen phase*), we use  $N$ -step self avoiding polygons (SAPs) on the cubic lattice, i.e. closed lattice walks whose steps can visit each vertex of the lattice at most once [23]. To mimic the quality of

the solvent we add to the model an effective attractive interaction potential which lowers the total energy by  $\epsilon = 1$  whenever two non-consecutive vertices of the SAP are one lattice distance apart. This attractive interaction is sufficient to induce a collapse transition at a critical temperature  $T_c$  and, for  $T < T_c$ , it is known to describe the *compact phase* [23]. In this work we have used  $T = 2.5$ , well below the value  $T_c \simeq 3.717$  [24, 25]. A collapsed configuration with  $N = 1000$  steps is shown in Fig. 1(a). Equilibrium configurations are sampled by Monte Carlo simulations based on two different algorithms, one for each equilibrium phase. In the swollen phase the algorithm uses the set of two-pivots moves i.e. non-local deformations that are known to sample efficiently unweighted polygons in  $Z^3$  [26].

In the compact phase the two-pivots algorithm is known to be inefficient [25] and in order to have good statistics in this regime we use the pruned enriched Rosenbluth method (PERM). This is a walk growing algorithm that has been shown to be quite effective in sampling compact self-avoiding walks [27]. Note that here the efficiency of the algorithm is mitigated by the fact that only closed chains, i.e. a small fraction of the whole set of linear chains, are accepted. Nevertheless this limitation is not very severe in the compact phase and we have been able to sample compact polygons with  $N$  ranging from 200 (680000 configurations) up to 1600 (220000 configurations). For this range of  $N$  the compact phase is characterized by a sufficiently high knotting probability and knot complexity [28]. This is not the case in the swollen phase where the knot population becomes non negligible only for large values of  $N$ . In this case, in order to have good statistics of knots, we sample configurations with  $N$  ranging from 1000 up to 200000.

### B. Computation of the writhe and identification of knots

A commonly used algorithm to compute the writhe of a curve goes as follows: First, one projects the curve onto an arbitrary plane. In general the projection will have crossings that most of the time will be transverse, so that, after having established an orientation of the curve, a sign  $+1$  or  $-1$  (determined by a right hand rule) can be assigned to each crossing. The sum of these signs gives the signed crossing number in this projection. The writhe of the curve is obtained by averaging these signed crossing numbers over all possible projections. From this definition it is clear that the main difficulty in computing the writhe of a configuration would be the averaging procedure over all projections. Fortunately, for polygons in  $Z^3$  this procedure is enormously simplified by a theorem [29] which reduces the writhe computation to the average of linking numbers of the given curve with four selected push-offs of the curve itself. In our calculation of the writhe we made extensive use of this result.

The determination of the knot type of a given config-

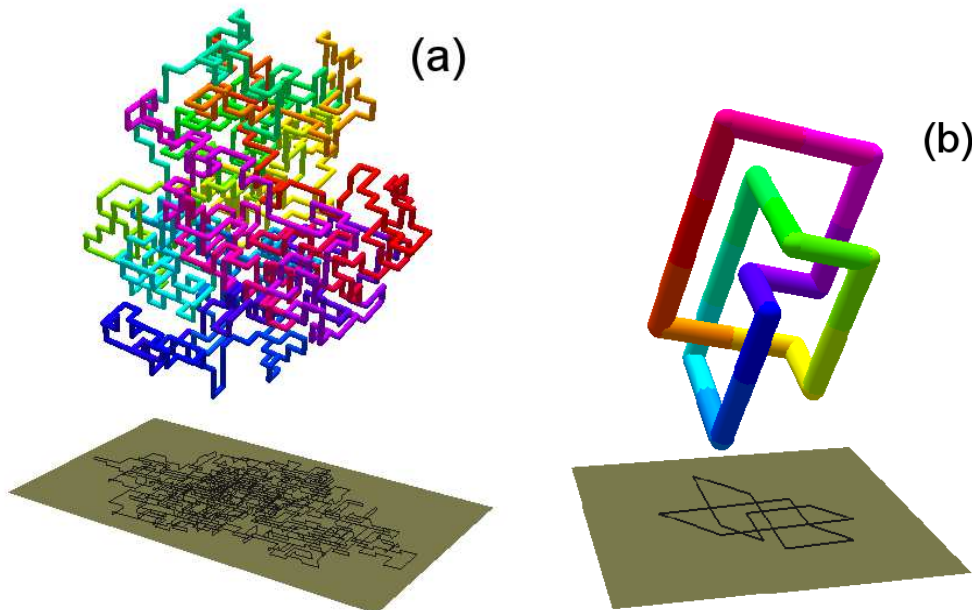


FIG. 1: (a) Example of a  $N = 1000$  steps compact configuration and its projection on a plane. (b) The configuration of Fig. 1(a) after the simplification procedure based on the BFACF algorithm. Note that in this case the simplification has been able to reach the minimal number of steps ( $N = 24$ ) compatible with the knot type  $(3_1)$  of the polygon [41].

uration, is in general, a difficult task both in the swollen phase where  $N$  is very large and in the compact phase where polygons are highly condensed. In both cases any projection of the chain onto a plane gives rise to a knot diagram with many crossings that makes the calculation of polynomial invariants quite prohibitive [see Fig. 1(a)]. To circumvent this difficulty, we simplify each sampled configuration before performing the projection. This is achieved by applying to the polygon a smoothing algorithm which progressively reduces the length of the chain while keeping its knot type unaltered (for a similar procedure, see [30]). This procedure is based on the BFACF algorithm [31, 32], an  $N$ -varying Monte Carlo method that is known to be ergodic within each knot type and in which the step fugacity, if kept low enough, induces a rapid reduction in the number of edges in the polygon. This simplification technique can reduce dramatically the number of crossings encountered in an arbitrary projection, as shown in Fig. 1(b) for the case of Fig. 1(a) and more generally in Fig. 2 for compact and swollen polygons with  $N = 1000$ . Note that the simplification procedure has a dramatic effect on the number of crossings.

For each simplified configuration we perform 500 projections and we choose the projection with the minimal number of crossings. The resulting knot diagram is encoded in terms of the Dowker code [33]. A further simplification of the Dowker code based on Reidemeister-like moves is performed. Finally, a factorization of the Dowker code is attempted. This procedure, whenever successful, splits composite knots into their prime components. From each component of the original Dowker

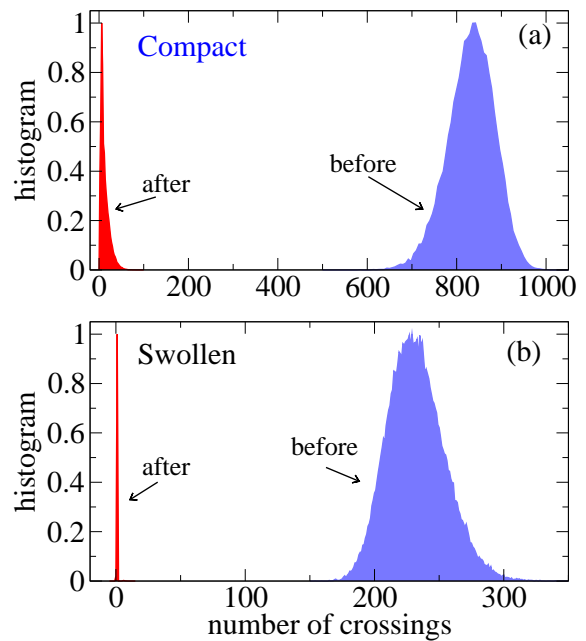


FIG. 2: Histogram (with arbitrary normalization) of the averaged (over 500 projections) number of crossings before and after the simplification procedure. Panels (a) and (b) refer to polygons with  $N = 1000$  respectively in the compact and swollen phase.

code we extract, by using KNOTFIND [34], the knot type of the original configuration. In this way we have been able to distinguish composite knots with up to 5 prime

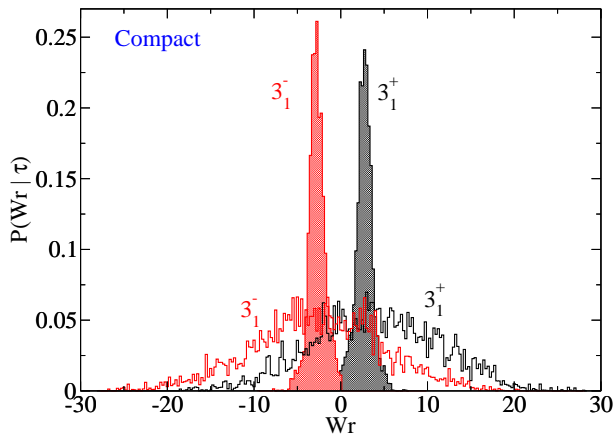


FIG. 3: The dense histogram is the distribution of the writhe after the simplification based on the BFACF algorithm for the knot type  $3_1$  ( $N = 1600$ ,  $T = 2.5$ ). This is divided in two sectors  $Wr \leq 0$  and  $Wr > 0$  to emphasize the detection of the two chiralities. Distributions of the writhe corresponding to original configurations for each chirality are shown as empty histograms. Bins have size  $1/4$ , i.e. the minimum resolution of  $Wr$  on the cubic lattice.

components, and with each component having crossing number up to 11.

To identify the chirality of a given knot type we cannot simply rely on the above procedure, since the Dowker code does not account for the handedness of the knot. Following [35] we used a heuristic approach based on the well known correlation between the chirality of a knot and the writhe of its minimal diagrammatic representation [10, 11]. This corresponds to computing the distribution of the writhe of the simplified configurations and looking at the shape of this distribution. If the distribution is sharply peaked around a well defined positive or negative value of the writhe one can assert with confidence that the knot is chiral with corresponding sign. In Fig. 3 we show the distribution of the writhe for the simplified configurations with a knot  $3_1$ , for  $N = 1600$  and  $T = 2.5$ . The distribution is clearly bimodal, and one can reliably distinguish most of the knot chiralities. Distributions of corresponding configurations before the BFACF procedure are also shown for comparison. Clearly the main uncertainties in this method of chiral detection are due to configurations whose writhe, after BFACF simplification, has a value close to zero. For these, relatively few, configurations we have calculated the Jones polynomial, and hence their chirality, explicitly.

### III. NUMERICAL RESULTS

#### A. The writhe distribution for fixed knot type

We first focus on the writhe distribution for configurations with fixed knot type  $\tau$ ,  $P_N(Wr|\tau)$ . In Fig. 4 and Fig. 5 we show the distributions  $P_N(Wr|\tau)$  for some

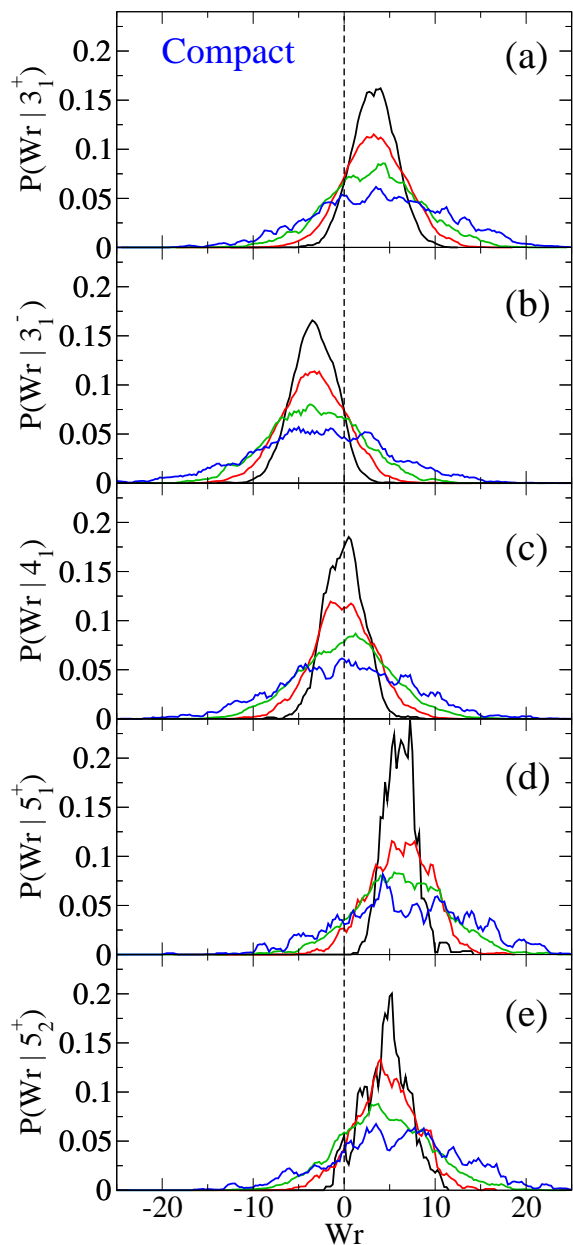


FIG. 4: Distributions  $P(Wr|\tau)$  in the compact phase for  $N = 200$  (narrower), 400, 800, and 1600: (a)  $\tau = 3_1^+$ , (b)  $3_1^-$ , (c)  $4_1$ , (d)  $5_1^+$ , and (e)  $5_2^+$ .

knots respectively in the compact and swollen phases. In each panel different curves correspond to different values of  $N$ . We stress again that, in the good solvent regime, the knot probability is very low unless  $N$  is large. Consequently we have to consider polygons with  $N$  values that are up to two orders of magnitude larger than their compact counterparts. For the  $3_1$  knot both mirror images are shown. The plots suggest a very small (if any) dependence on  $N$  for the average writhe  $\mu(\tau)$  whereas as  $N$  increases the distributions tend to broaden. This behavior, already observed in [10, 11] for swollen polygons is here confirmed also for compact configurations. The dif-

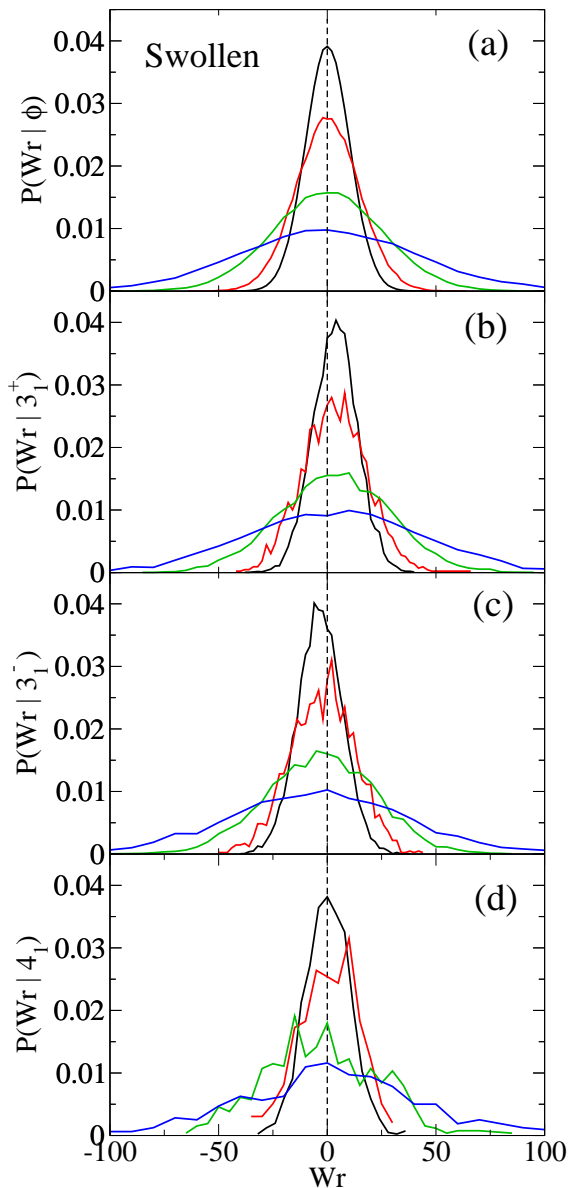


FIG. 5: Distributions  $P(Wr|\tau)$  in the swollen phase for  $N = 5000$  (narrower), 10000, 30000, and 80000: (a) unknot (b)  $\tau = 3_1^+$ , (c)  $3_1^-$ , (d)  $4_1$ .

ferent ranges in  $Wr$  between swollen and compact phases are due to the different values of  $N$  considered in the two situations. If the same value of  $N$  is considered (see Fig. 6 for  $N = 1000$ ) the distribution  $P_N(Wr|\tau)$  looks similar in the two phases, being slightly broader for compact polygons.

In Fig. 7 we show the writhe distribution for achiral compact polygons for  $N = 1600$ : all the curves are symmetric and centered around zero. It was shown rigorously in [10] that achiral knots have mean writhe equal to zero for un-weighted polygons. That argument is a symmetry argument that can be extended *mutatis mutandis* to the case of compact polygons.

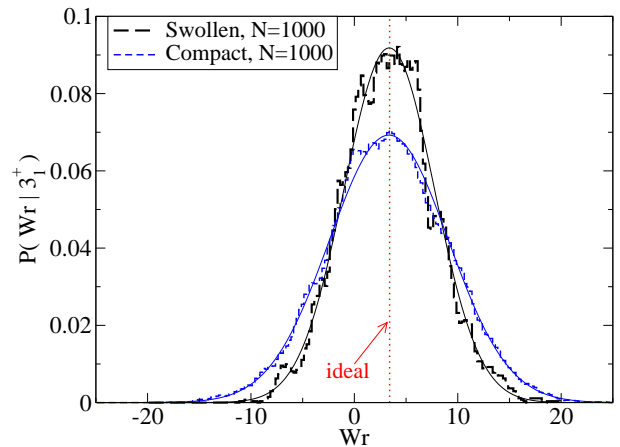


FIG. 6: Distributions  $P(Wr|\tau)$  for polygons with  $N = 1000$ , both in the swollen (thick dashed line) and in the compact (dashed line) phase. The thin solid lines correspond to one parameter Gaussian fits in which the value of the average is fixed to the ideal value  $\mu(3_1^+) \simeq 3.41$ .

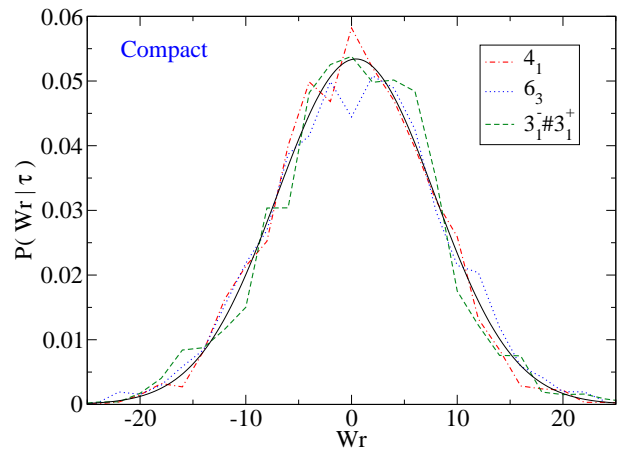


FIG. 7: Distributions  $P(Wr|\tau)$  for polygons with  $N = 1600$  in the compact phase, for achiral knots  $\tau = 4_1$  and  $\tau = 6_3$ , and for a composite achiral knot  $\tau = 3_1^- \# 3_1^+$ . The solid line is a one parameter Gaussian fit with zero mean.

In Fig. 8 we report the  $N$  dependence of the average writhe for different knot types, respectively in the compact and swollen phase. Within error bars (68% confidence intervals) it is clear that the average writhe is essentially independent of  $N$  and the values are in good agreement with those calculated previously for different models of polymers in good solvent [8, 9] and for ideal knots [11, 12] (dashed lines in the plots). The agreement between the average writhe for a fixed knot type  $\tau$  and the value for the corresponding ideal knot is extended to composite knots as shown in Fig. 9 indicating that the additivity property of the writhe under knot composition found for ideal knots in [36] and for unweighted polygons in [10] applies also for the case of compact polygons. In fact Sumners [37] has recently proved a result about additivity of writhe under the connect sum operation for

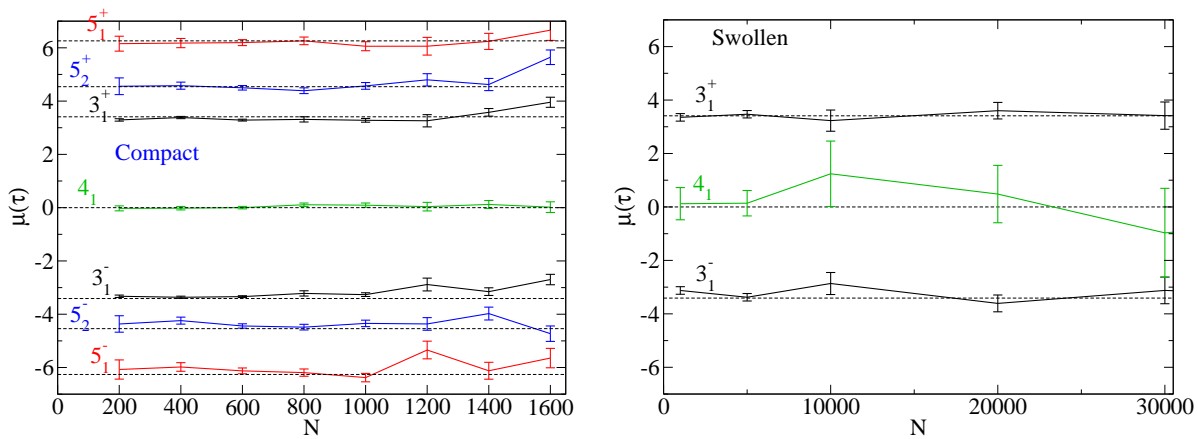


FIG. 8: Mean writhe for several knots in the compact (left panel) and swollen (right panel) phase. Dashed lines are the values of corresponding ideal knots

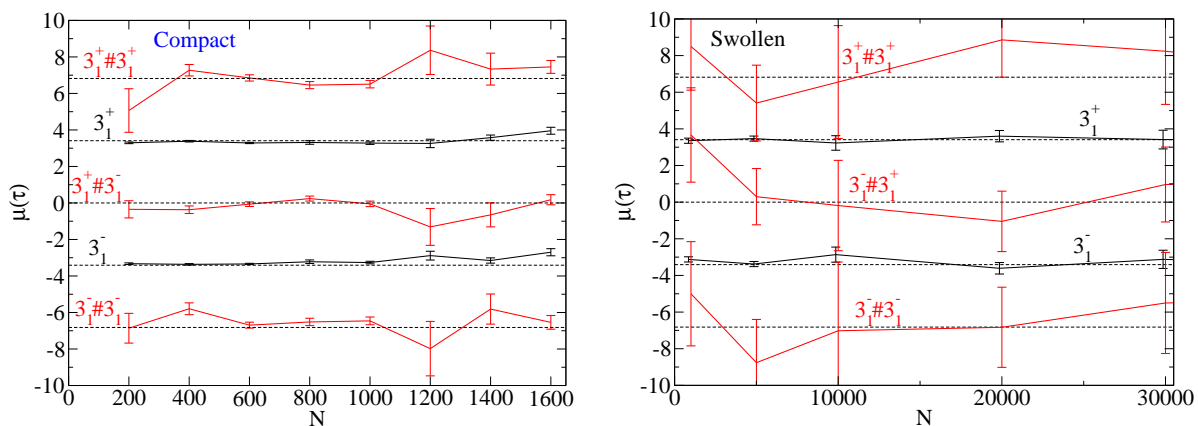


FIG. 9: Mean writhe for knots  $3_1$  and all the possible composite knots  $3_1 \# 3_1$  in the compact (left panel) and swollen (right panel) phase. Dashed lines are the values of the sum of the means writhe of the corresponding ideal prime knots.

unweighted polygons.

The fact that the average writhe is independent of the quality of the solvent is a further indication that this number reflects topological properties of the rings no matter how badly they are embedded in space. One can understand this property by the following argument: for a given configuration and projection one may attempt to simplify the resulting knot diagram by performing Reidemeister moves with the goal of removing most of the inessential crossings. This will give a diagram with the minimal number of crossings compatible with the projection and with the given knot type  $\tau$ . Note that in the cubic lattice this procedure would correspond to a simplification of the original configuration for example by using the BFACF algorithm. This will bring the original configuration, either swollen or compact, close to the one with the minimal number of steps (ideal configuration on the cubic lattice). Let us now see how this procedure affects the average writhe  $\mu(\tau)$ . Since the Reidemeister II and Reidemeister III moves always involve pairs of crossings with opposite signs, the planar writhe is unaf-

fected. This is not true for the first Reidemeister move that removes single crossings. For a particular conformation the number of crossings with positive and negative signs that can be removed by Reidemeister I moves will not be equal. However, the procedure of averaging over all conformations should drastically reduce this average difference. The resulting average planar writhe is then related to the essential crossings for a given knot type and should coincide with the value for the ideal knot. Note that the above arguments suggest that the distribution  $P_N(Wr|\tau)$  has Gaussian tails. In fact if the knot is achiral (as in Fig. 7) or if chiral knots are split into mirror components (as for example the plus trefoil in Fig. 6), the writhe distribution turns out to be well approximated by a Normal distribution  $\mathcal{N}(\mu(\tau), \sigma(\tau))$  with mean  $\mu(\tau)$  and standard deviation  $\sigma(\tau)$  (see solid lines in Fig. 6 and Fig. 7).

By looking at the width of the distributions in Figures 4 and 5 it is clear that the standard deviation  $\sigma_N(\tau)$  increases with  $N$  and this dependence is shown in Fig. 10, left panel, for compact prime knots and for swollen knots

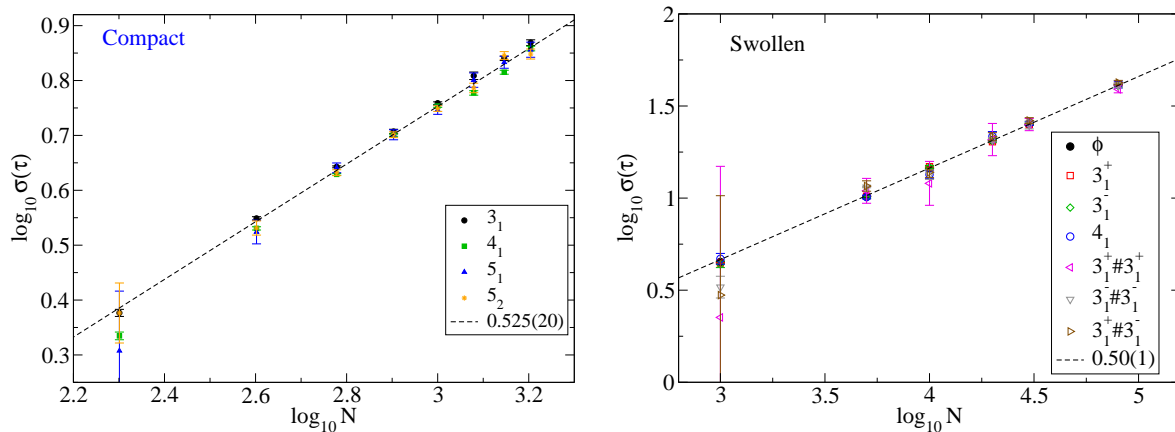


FIG. 10: Log-log plot of the standard deviation  $\sigma_N(\tau)$  of the writhe distribution, as a function of  $N$ , for several knots (averaged over mirror images), in the compact (left panel) and swollen (right panel) phase. For each knot type the data have been fit by a power law of the form  $A(\tau)N^{\eta_\tau}$  (dashed lines) with  $\eta_\tau = 0.525 \pm 0.020$  in the compact phase and  $\eta_\tau = 0.50 \pm 0.01$  in the swollen one. Note that for compact polygons, in order to avoid correction to scaling effects, the fit has been obtained by excluding the data  $N = 200, 400$ .

in the right panel. A simple fit of the data in the form  $A(\tau)N^{\eta_\tau}$  gives estimates of the exponents that, within error bars, are independent on the knot type  $\tau$  and whose value is  $0.525 \pm 0.020$  for compact polygons and  $0.50 \pm 0.01$  for swollen ones. Note that the two values are, within error bars, compatible suggesting that  $\eta_\tau$  is also independent of the equilibrium phase, and possibly equal to  $1/2$ .

Given that  $\eta_\tau$  seems to be independent of  $\tau$  it is interesting to see if this is also the case for the amplitude  $A(\tau)$ . In Fig. 11 we plot  $\sigma_N(\tau)/N^{\eta_\tau}$  for different knot types, respectively in the compact (left panel) and swollen (right panel) phase. Within error bars the amplitude turns out to be independent of the knot type.

It is interesting to compare the  $N$  dependence of  $\sigma_N(\tau)$  [i.e. the standard deviation of the distributions  $P_N(Wr|\tau)$ ] with the one,  $\sigma_N$ , that measures the broadness of  $P_N(Wr) = \sum_\tau \pi_N(\tau)P_N(Wr|\tau)$  where  $\pi_N(\tau)$  is the probability of occurrence of knot type  $\tau$ . Note that  $P_N(Wr)$  is the writhe distributions of the whole set of polygons. In Fig. 12 we plot  $\sigma_N$  as a function of  $N$  for swollen (empty circles) and compact (empty squares) polygons. Moreover, since often in the literature, the width of the writhe distribution  $P_N(Wr)$ , is described in terms of the mean of the absolute value of the writhe  $\langle |Wr| \rangle_N$ , in Fig. 12 we have also reported this quantity in terms of solid symbols. The plots are on a log-log scale and the linear behavior suggests a power law dependence  $AN^\eta$ . Note that for each phase solid and empty symbols lie on parallel lines indicating that  $\sigma_N$  and  $\langle |Wr| \rangle_N$  display the same power law behavior but different amplitude. A simple linear fit of the data furnishes the estimate  $\eta = 0.5035 \pm 0.0006$  in the swollen phase and  $\eta = 0.599 \pm 0.002$  in the compact one. The value found for the swollen regime agrees with previous estimates [38] and is close to the rigorous lower bound  $1/2$  established for  $\langle |Wr| \rangle$  [38]. In the compact phase, however, the expo-

nent  $\eta$  is significantly higher than its swollen counterpart but markedly smaller than the rigorous upper bound  $4/3$  found in [39]. Its value is also smaller than  $0.75$ , i.e. the one estimated in [30], for Gaussian chains confined in small spheres. The difference between these two last estimates could be due to the presence, in our case, of the excluded volume interactions that increase the persistence length of the chain making the wrapping of the chain around itself more costly. However, the difference in the value of  $\eta$  could be due to a difference in the spatial organization of compact configurations obtained by self-attraction compared to the ones obtained by a severe geometrical confinement.

An important byproduct of the analysis of  $\sigma_N$  and  $\sigma_N(\tau)$  is that  $\eta \approx \eta_\tau$  in the swollen phase whereas  $\eta > \eta_\tau$  in the compact one. This should be contrasted with the fact that  $\eta_\tau$  is nearly the same  $\simeq 1/2$  in the two phases.

A possible explanation of this striking behavior may be that the writhe of a given configuration can be decomposed into a “geometrical” contribution coming from the spatial organization of the polygon and the topological one coming purely from the knot type of the configuration. For the swollen case it is known that the geometrical contribution to  $\sigma$  increases at least as rapidly as  $\sqrt{N}$  which is what was found for the set of all polygons in the swollen phase. In this phase, the topological contribution apparently does not scale faster than  $\sqrt{N}$ . In general however the situation could be different since a sum over all knot types must be taken into account and the topological contribution could become important if the probability of a knot type  $\tau$  to occur, i.e.  $\pi_N(\tau)$  is sufficiently large. This turns out to be the case for compact polygons where the knotting probability increases with  $N$  with an exponential factor that is a factor of 1000 bigger than for its swollen counterparts.

To make these arguments more precise let us suppose that  $P_N(Wr|\tau)$  are well approximated by Gaussian dis-

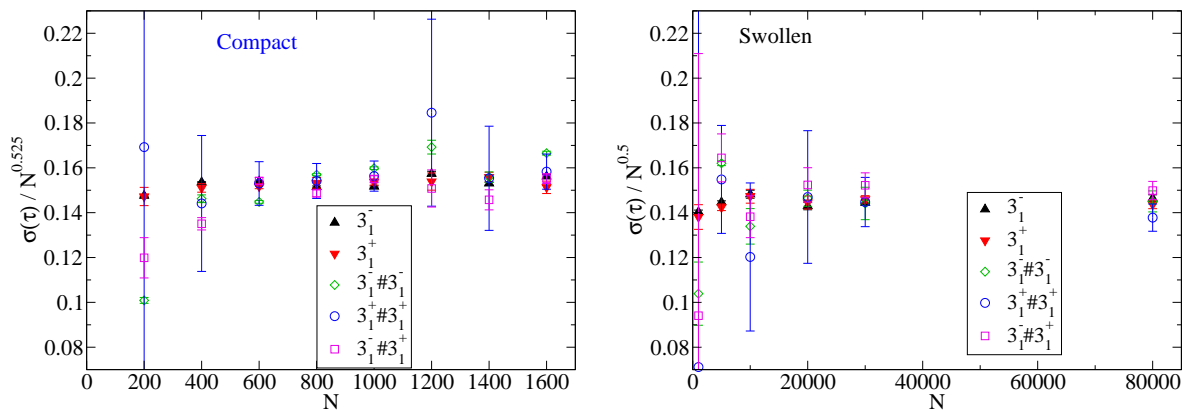


FIG. 11: Standard deviation  $\sigma(\tau)$  divided by  $N^{\eta_\tau}$  for different knot types in the compact (left panel) and swollen (right panel) phase. The value of  $\eta_\tau$  considered is  $0.525 \pm 0.020$  for compact polygons and  $0.50 \pm 0.01$  for the swollen ones.

tributions. If this is the case (as suggested by our results) the conditional distributions  $P_N(Wr|\tau)$  are completely defined by the average  $\mu_N(\tau)$  and the standard deviation  $\sigma_N(\tau)$ . If knots are distinguished by chirality, clearly the variance of the distribution is  $\sigma_N(\tau)^2$ . If we sum over the mirror images the mean writhe is zero and the overlap of two Gaussian distributions implies that  $\langle Wr^2 \rangle_N(\tau) = \sigma_N(\tau)^2 + \mu_N(\tau)^2$ . This term is for fixed knot type and, in order to compute the global second moment, the term must be weighted by the probability of occurrence of the knot

$$\langle Wr^2 \rangle = \sum_{\tau} \pi_N(\tau) \langle Wr^2 \rangle_N(\tau).$$

This gives

$$\langle Wr^2 \rangle = \langle \sigma_N(\tau)^2 \rangle + \langle \mu_N(\tau)^2 \rangle.$$

The scaling of  $\langle Wr^2 \rangle$  depends on whether  $\langle \sigma^2 \rangle$  or  $\langle \mu^2 \rangle$  increases more rapidly as  $N$  increases. For the compact case it seems that  $\langle \mu^2 \rangle$  increases more rapidly than  $\langle \sigma^2 \rangle$  while this is not true in the swollen phase. We can estimate  $\langle \mu_N(\tau)^2 \rangle$  in the swollen phase by using the ideal  $\mu_N(\tau)$  whenever a knot  $\tau$  contributes to the statistics. Since the two members of a chiral pair occur with roughly equal probabilities and since knots are weakly localized in the swollen phase we can estimate the writhe of a composite knot (for all chiral combinations) by assuming independence. The average  $(\langle \mu_N(\tau)^2 \rangle)^{1/2}$  from this analysis turns out to scale  $\sim \sqrt{N}$ , see Fig. 12, and with an amplitude much smaller than  $\sigma_N$ , confirming that the scaling of  $\sigma_N$  is governed by the geometrical spread  $\langle \sigma_N(\tau)^2 \rangle$  of all knots around their ideal value.

Hence, the important difference between the swollen phase and the compact one is that collapsed polymers display a rich spectrum of knots  $\pi_N(\tau)$  for moderate lengths  $N$  [28], while in good solvent conditions knots start to appear with a non-negligible frequency only for  $N \gtrsim 10^5$  [40]. At that stage  $\sigma(\tau) \gg |\mu(\tau)|$  and hence  $\langle Wr^2 \rangle_N(\tau) \simeq \sigma(\tau)^2$ . On the contrary, in the compact

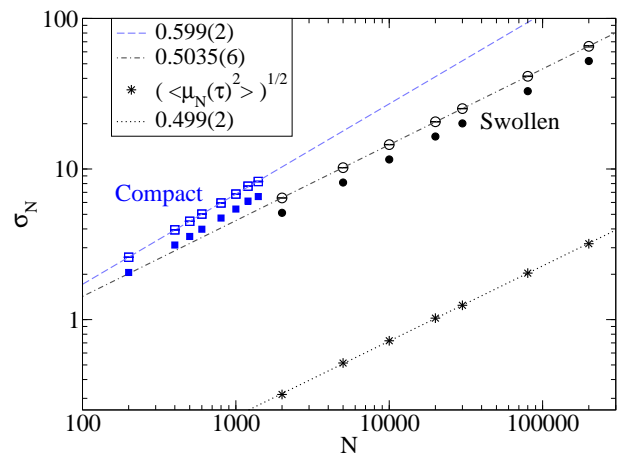


FIG. 12: Log-log plot of  $\sigma(\tau)$  vs  $N$  in the swollen phase (circles) and in the compact phase (squares). The filled symbols refer to the mean of the absolute value of the writhe. Dashed lines are the result of a linear fit and have a slope of  $0.599 \pm 0.002$  and  $0.5035 \pm 0.0006$  respectively for compact and swollen polygons. Stars refer to the average square of the mean value of writhe of knots in the swollen phase and the dotted line is a fit with slope  $0.499 \pm 0.002$ .

phase knots start to appear with a non-negligible frequency already for  $N$ 's where  $|\mu(\tau)| \gtrsim \sigma(\tau)$ , in which case  $\langle Wr^2 \rangle_N(\tau) \simeq \mu(\tau)^2$  is a good approximation. Because of this effect, the global  $\langle Wr^2 \rangle$  has a scaling that does not trivially follow that of single knots.

## B. Knot spectrum at fixed writhe

Podtelezchnikov *et al* [8] have investigated the probability of finding a specific knot type, conditioned on the writhe, for a model of circular DNA in a good solvent. In this section we examine how the presence of writhe might affect the knot spectrum in the swollen and compact phases. The idea is to



extract a subset of the sample of polygons whose writhe falls into a window of values  $[Wr_{\min}, Wr_{\max}]$ . Within this subset one looks at the relative frequency of occurrence of a given knot. This corresponds to estimating the probability  $P(\tau|[Wr_{\min}, Wr_{\max}]) = \int_{Wr_{\min}}^{Wr_{\max}} P(\tau|Wr) / \sum_{\tau} \int_{Wr_{\min}}^{Wr_{\max}} P(\tau|Wr)$ . In Fig. 13 we plot the knot spectrum for two different intervals of the writhe (middle and lower panels) for polygons in the compact phase. The top panel is the knot spectrum obtained by summing over all values of the writhe and is shown as a reference. Let us focus first on the  $N = 600$  case (empty bars). Here it is clear that, as writhe increases, the knot spectrum changes dramatically with respect to the case of unconstrained writhe (top panel). In particular one sees that in configurations with relatively large value of writhe (bottom panel) the achiral knot  $4_1$  is practically suppressed and that the torus knot  $5_1$  becomes more frequent than the twist knot  $5_2$ . This is an effect that was previously found for almost ideal configurations [8, 9] and for polymers confined in spheres [18]. Here it is extended to the case of random self-attracting polymers in the collapsed phase.

In previous sections we have shown that the average writhe of a given knot is insensitive to changes in  $N$ . It thus makes sense to use the same windows  $[Wr_{\min}, Wr_{\max}]$  for any comparison between results for different  $N$ 's. On the other hand, we have seen that the variance  $\sigma_N(\tau)^2 \sim N$  indicating that writhe distributions for contiguous (in complexity) knots will have an overlap that becomes more and more important as  $N$  increases. Hence, a windowing procedure should be less efficient in picking up a given subset of knots. This is indeed the case, for compact polygons with  $N = 1400$  (filled histograms in Fig. 13). For  $N = 1400$  the values of the writhe considered do not show the writhe bias effect on the knot spectrum because the writhe distributions of the knots considered are not well separated.

In the swollen phase, the conditional distributions  $P(\tau|Wr)$  of different knots can be of comparable magnitude in a window of values  $[Wr_{\min}, Wr_{\max}]$  only for very large  $N$ , because knots are rare for short chains. For long chains,  $P(\tau|Wr)$  is essentially a broad Gaussian with average much smaller than its standard deviation, and of course with normalization  $\sim P(\tau)$ . Hence, in a window  $[Wr_{\min}, Wr_{\max}]$  one just normally finds that  $P(\tau|[Wr_{\min}, Wr_{\max}]) \sim P(\tau)$ , that is, no sensible dependence on the writhe interval is present.

#### IV. CONCLUSIONS

We have investigated with Monte Carlo methods the interplay between writhe and knotting in ring polymers in both good and poor solvent conditions. To model good solvent conditions we used self-avoiding polygons on the simple cubic lattice and we incorporated an attractive interaction between neighboring pairs of vertices to model poor solvent conditions, leading to compact configura-

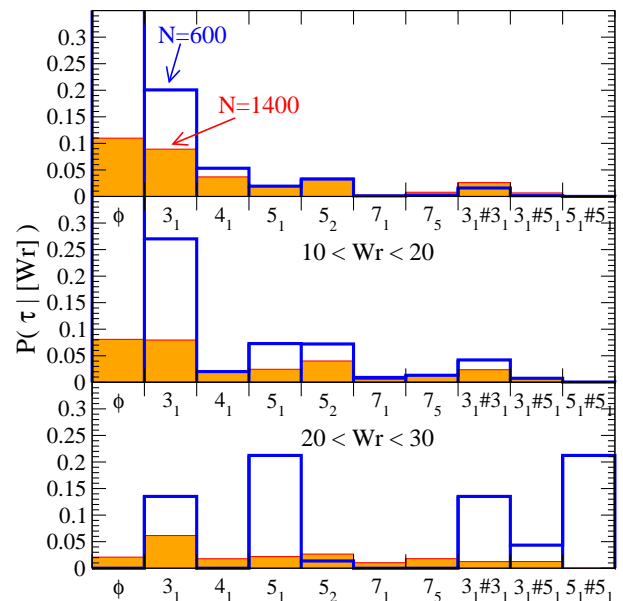


FIG. 13: Frequency of some knots, regardless of the writhe (upper panel), for compact configurations with  $10 < Wr < 20$  (central panel), and  $20 < Wr < 30$  (lower panel), both for  $N = 600$  (empty histogram) and for  $N = 1400$  (dense histogram).

tions.

For polygons with fixed knot type we computed the writhe distribution. The mean writhe is zero for achiral knots while for chiral knots it is non-zero but is insensitive to the length of the polygon. This has been observed previously for the good solvent case but we observe the same effect for poor solvents. Moreover, for each knot type, both mean values are consistent with that of ideal knots.

In the swollen case, the width of the writhe distribution increases as the square root of the length of the chain. Within errors, this is true also in the collapsed phase. On the other hand, the mean spread of the writhe computed without distinguishing knots scales differently (with exponent  $\simeq 0.6$ ) for compact polymers. The reason is that, in this regime, the population of knots grows quickly with the chain length, including complex knots with large mean writhe values. Therefore, the swollen phase is characterized by the geometrical spread of configurations, while the statistics of writhe in the compact regime is governed by the topological contribution of the mean writhe of knots.

Finally, we have observed that picking up a specific knot by constraining the writhe in a given window is not possible if the chain length is much longer than the persistence length of the polymer.

It is well known that the mobility of a circular DNA molecule in gel electrophoresis is sensitive to the writhe of the molecule. If the circular DNA is prepared with a particular knot type then this type of experiment could be used, in principle, to measure the mean writhe and

determine how the writhe is related to the knot type. By changing the ionic strength of the solution the typical dimensions of the molecule could be changed, in an analogous way to changing solvent quality.

## V. ACKNOWLEDGMENT

E.O. was supported by a grant from MIUR-PRIN05. S.G.W. acknowledges financial support from NSERC.

M.B. acknowledges financial support from K. U. Leuven under Grant No. OT/07/034A and from University of Padua and Progetto di Ateneo n. CPDA083702.

- 
- [1] J. D. Watson and F. H. Crick, *Nature* **171**, 737 (1953).
- [2] J. H. White, *American Journal of Mathematics* **91**, 693 (1969), ISSN 00029327.
- [3] F. B. Fuller, *Proc Natl Acad Sci U S A* **68**, 815 (1971).
- [4] W. R. Bauer, *Annu. Rev. Biophys. Bioeng.* **7**, 287 (1978).
- [5] S. Y. Shaw and J. C. Wang, *Science* **260**, 533 (1993).
- [6] V. V. Rybenkov, N. R. Cozzarelli, and A. V. Vologodskii, *Proc. Natl. Acad. Sci. USA* **90**, 5307 (1993).
- [7] K. Shishido, N. Komiyama, and S. Ikawa, *J. Mol. Biol.* **195**, 215 (1987).
- [8] A. A. Podtelevnikov, N. R. Cozzarelli, and A. V. Vologodskii, *Proc. Natl. Acad. Sci. USA* **96**, 12974 (1999).
- [9] Y. Burnier, J. Dorier, and A. Stasiak, *Nucleic Acids Res.* **36**, 4956 (2008).
- [10] E. J. Janse van Rensburg, E. Orlandini, D. W. Sumners, M. C. Tesi, and S. G. Whittington, *J. Knot Th. Ramif.* **6**, 31 (1997).
- [11] V. Katritch, J. Bednar, D. Michoud, J. Dubochet, and A. Stasiak, *Nature* **384**, 142 (1996).
- [12] A. Stasiak, V. Katritch, and L. H. Kauffman, eds., *Ideal Knots* (World Scientific Publishing, Singapore, 1998).
- [13] A. Flammini and A. Stasiak, *Proc. Royal Soc. A* **463**, 569 (2007).
- [14] L. F. Liu, J. L. Davis, and R. Calendar, *Nucleic Acids Res.* **9**, 3979 (1981).
- [15] J. S. Wolfson, G. L. McHugh, D. C. Hooper, and M. N. Swartz, *Nucleic Acids Res.* **13**, 6695 (1985).
- [16] M. Isaksen, B. Julien, R. Calendar, and B. H. Lindqvist, *Methods Mol. Biol.* **94**, 69 (1999).
- [17] J. Arsuaga, M. Vázquez, S. Trigueros, D. Sumners, and J. Roca, *Proc. Natl. Acad. Sci. USA* **99**, 5373 (2002).
- [18] J. Arsuaga, M. Vazquez, P. McGuirk, S. Trigueros, D. Sumners, and J. Roca, *Proc. Natl. Acad. Sci. USA* **102**, 9165 (2005).
- [19] K. Murray and N. E. Murray, *Nat. New Biol.* **243**, 134 (1973).
- [20] V. V. Rybenkov, C. Ullsperger, A. V. Vologodskii, and N. R. Cozzarelli, *Science* **277**, 690 (1997).
- [21] S. Trigueros and J. Roca, *BMC Biotechnol.* **7**, 94 (2007).
- [22] T. Blackstone, P. McGuirk, C. Laing, M. Vazquez, J. Roca, and J. Arsuaga, in *Proceedings of the conference on knots in Kyoto 2007* (Osaka University Press, 2009), ch. 18.
- [23] C. Vanderzande, *Lattice Models of Polymers* (Cambridge University Press, Cambridge, UK, 1998).
- [24] M. C. Tesi, E. J. Janse van Rensburg, E. Orlandini, and S. G. Whittington, *J. Stat. Phys.* **82**, 155 (1996).
- [25] M. C. Tesi, E. J. Janse van Rensburg, E. Orlandini, and S. G. Whittington, *J. Phys. A.* **29**, 2451 (1996).
- [26] N. Madras and G. Slade, *The Self-Avoiding Walk* (Birkhäuser, 1993).
- [27] P. Grassberger, *Phys. Rev. E* **56**, 3682 (1997).
- [28] M. Baiesi, E. Orlandini, and A. L. Stella, *Phys. Rev. Lett.* **99**, 058301 (2007).
- [29] R. C. Lacher and D. W. Sumners, in *Computer Simulation of Polymers*, edited by R. Roe (Prentice-Hall, New York, 1991), pp. 365–373.
- [30] C. Micheletti, D. Marenduzzo, E. Orlandini, and D. W. Sumners, *J. Chem. Phys.* **124**, 064903 (2006).
- [31] B. Berg and D. Foerster, *Phys. Lett. B* **106**, 323 (1981).
- [32] C. Aragao de Carvalho, S. Caracciolo, and J. Fröhlich, *Nucl. Phys. B* **215**, 209 (1983).
- [33] C. C. Adams, *The Knot Book* (Freeman, 1994).
- [34] J. Hoste and M. Thistlethwaite (1999), URL <http://www.math.utk.edu/morwen/knotscape.html>.
- [35] C. Micheletti, D. Marenduzzo, E. Orlandini, and D. W. Sumners, *Biophys. J.* **95**, 3591 (2008).
- [36] V. Katritch, W. K. Olson, P. Pieranski, J. Dubochet, and A. Stasiak, *Nature* **388**, 148 (1997).
- [37] D. Sumners (2009), talk given at the San Francisco International Meeting on DNA Topology.
- [38] E. J. Janse van Rensburg, E. Orlandini, D. W. Sumners, M. C. Tesi, and S. G. Whittington, *J. Phys. A: Math. Gen.* **26**, L981 (1993).
- [39] J. Cantarella, D. DeTurk, and H. Gluck, in *Proc. of the Conference on Low dimensional Topology in Honor of the 70th birthday of Joan Birman* (Amer. Math. Soc. International, Sommerville, MA, 2002), vol. 24.
- [40] E. Orlandini and S. Whittington, *Rev. Mod. Phys.* **79**, 611 (2007).
- [41] Y. Diao, *J. Knot Th. Ramif.* **2**, 413 (1993).